

**Shell-thickness control of hollow SiO<sub>2</sub> nanoparticles through post-treatment using sol–gel technique toward efficient water confinement.**

*Naoki Tarutani<sup>a,b,c,\*</sup>, Yuka Honda<sup>b</sup>, Risa Hamakawa<sup>b</sup>, Tetsuo Uchikoshi<sup>c,d</sup>, Takamasa Ishigaki<sup>b,c\*</sup>*

<sup>a</sup> Applied Chemistry Program, Graduate School of Advanced Science and Engineering, Hiroshima University, 1-4-1 Kagamiyama, Higashi-Hiroshima, Hiroshima 739-8527, Japan.

<sup>b</sup> Department of Chemical Science and Technology, Faculty of Bioscience and Applied Chemistry, Hosei University, 3-7-2 Kajino-cho, Koganei, Tokyo 184-0003, Japan.

<sup>c</sup> Research Center for Micro-Nano Technology, Hosei University, 3-11-15 Midori-cho, Koganei, Tokyo 184-8584, Japan.

<sup>d</sup> Research Center for Functional Materials, National Institute for Materials Science, 1-2-1, Sengen, Tsukuba, 305-0047, Japan.

\* E-mail addresses of corresponding authors: n-tarutani@hiroshima-u.ac.jp, ishigaki@hosei.ac.jp

Keywords: hollow nanoparticles, sol–gel reaction, water confinement, nanocomposites

**ABSTRACT:** Hollow structures possess a confinement function, which enables the handling and use of functional liquids. In this study, we focus on the confinement of water in the inner spaces of hollow SiO<sub>2</sub> nanoparticles (HSNPs). Water is introduced into the hollow spaces after passing through the mesopores of the shells. The introduced water is then confined by thickening the shell through a post-treatment using silicon alkoxides. HSNPs with a variety of shell thicknesses are prepared by tuning the synthetic conditions of the reaction media and the alkoxides. It is found that the amount of water retained in a hollow space is increased with shell thickness. The resultant water–H SNP nanocomposites exhibit effective far-infrared absorption. The facile confinement approach reported in this study will lead to highly functional complex nanocomposites, such as isolated metal nanoparticles–water–silica.

## 1. Introduction

Structuration provides materials with extrinsic as well as intrinsic properties.[1] For example, hollow structures provide materials with a heat insulating function, which leads to application in many fields, as energy,[2,3] thermal,[4] biological, and optical materials.[5,6] The hollow structures are generally fabricated using template materials,[7] such as polystyrene,[8,9] calcium carbonate,[10,11] and hydroxyapatite.[12] Compared with template-free processes,[13,14] the templating process has certain advantages, such as allowing for the size, shape, and morphology of the hollow structures to be tuned.[15] Such hollow structures influence various functions, such as the mechanical,[16] thermal,[17] biological,[18] and optical properties.[19,20] Another advantage of templated hollow structures is the confinement of substances in the hollow spaces to form composites.

Hollow materials prepared using templates have numerous inherent micro/mesopores in their shells as a result of removing the templates.[11,12] Gas and liquid species can be introduced to fill the inner hollow space through the micro/mesopores, which results in highly functional nanocomposites. Although mesoporous materials are known to be efficient adsorbents of various species, owing to their high specific surface area and large pore volume, molecules may become trapped at the mesowalls and retard diffusion,[21–23] which will limit the control of uptake and release kinetics. Among the combinations of hollow structured materials and confined substances, we focus on hollow SiO<sub>2</sub> nanoparticles (HSNPs) containing water in the context of smart optical materials.

Far-infrared (FIR) light from sunlight is one of the largest contributors of heating and governs the sensory temperature of humans. Transient receptor potential vanilloid 3 and 4 in keratinocytes release adenosine triphosphate, which is a messenger molecule for thermotransduction in skin.[24] FIR light is known to penetrate and be highly absorbed to a depth of approximately 200 μm from the skin surface,[25] where keratinocytes are located. Therefore, FIR light will trigger thermotransduction by messenger molecules and result in

increasing the sensory temperature. Water is an efficient FIR absorber.[26] A water layer will effectively reduce the FIR from sunlight even with a thickness on the  $\mu\text{m}$ -scale.[27,28] It is also expected that evaporation of water by FIR absorption will occur to conduct heat from the matrixes and body to further control the temperature. Using HSNPs as nanocontainers of water will lead to the fabrication of visible-light transmissive and FIR absorptive nanocomposites, which can be used in various applications such as temperature controlling windows and cosmetics.

This study focuses on a method to prepare HSNPs encapsulating controlled amounts of water. HSNPs with a size of less than 100 nm were employed as pristine nanoparticles. Among the various templates used toward the synthesis of HSNPs, calcium carbonates are ideal. The calcium carbonate templates can be removed by acid treatment and such a thermally mild treatment allows numerous mesopores to be left in the shells,[29] as opposed to thermally decomposing templates which sometimes leave macropores and/or collapsed hollow structures that are difficult to cover completely.[30] Water molecules penetrated the shell of the HSNPs through mesoscale pores and were introduced into the hollow spaces. The shells of HSNPs were thickened through post-treatment using the sol-gel technique. Tuning the synthetic parameters of the reacting media composition, precursor alkoxide molecular structure, and alkoxide concentration enabled control of shell growth. It was found that the confined amount of water molecules in the hollow space could be controlled by precisely tuning the thickness of the HSNP shells, which enabled efficient absorption of FIR. The solution confining HSNP nanocomposites are useful not only for the space for FIR adsorption, but also for the synthetic space of the isolated nanoparticles, like as plasmon-based functional metal nanoparticles[31]. The facile approach of confinement shown in this study will lead to the synthesis of highly functional and complex nanocomposites.

## **2. Materials and Methods**

## 2.1. Chemicals

HSNP powder (SiliNax) was purchased from Nittetsu Mining Co., Ltd (Japan). Tetramethyl orthosilicate (TMOS, 99%), tetraethyl orthosilicate (TEOS, 97%), tetrapropyl orthosilicate (TPOS, 98%), and tetrabutyl orthosilicate (TBOS, 98%) were purchased from Tokyo Chemical Industry Co. (Japan), Ltd. Ethanol (99.5%) and ammonium hydroxide solution (28 wt.%) were purchased from FUJIFILM Wako Pure Chemical Co. (Japan). Ultrapure water of 18.2 M $\Omega$ ·cm resistivity was used in all experiments. All reagents were used as received.

## 2.2. Shell-thickness control of HSNPs in ethanol-rich reaction conditions

HSNP powders (0.3 g) were dispersed in 10 mL of water and degassed for 20 min to introduce water into the hollow space of the nanoparticles. The water-containing HSNPs were collected by suction filtration and allowed to dry for 30 min at room temperature. Then, 0.1 g of the obtained powders was redispersed in 5 mL of ethanol and mixed with ethanolic solution (13.65 mL of ethanol and 1.35 mL of ammonium hydroxide solution). Immediately after mixing, 100  $\mu$ L of TEOS was added while stirring. Powders were collected by centrifugation (12557  $\times g$  for 20 min) after 20 h of stirring and were dried at 80  $^{\circ}$ C for 3 h.

## 2.3. Shell-thickness control of HSNPs in water-rich reaction conditions

HSNP powders (0.25 g) were dispersed in ammonium hydroxide solution (1.0 mol L $^{-1}$ , 50 mL) and ultrasonicated for 5 min to introduce water into the hollow space of the HSNPs. Specific amounts of alkoxide solutions (molar ratio of alkoxide:ethanol = 1:100) were added and the solutions were stirred for 20 h. The particles were separated by centrifugation at 12557  $\times g$  for 20 min and washed with ethanol twice. The sample prepared by this approach is denoted as x-y, where x is the kind of alkoxide employed (TMOS, TEOS, TPOS, and TBOS) and y is the millimole amount of alkoxide ( $y = 1.73, 2.60, 3.46, 3.90, 4.33,$  and 6.50).

## 2.4. Characterization

A field emission scanning electron microscope (SEM) (SU8020, Hitachi High-Technologies Corp., Japan) equipped with a scanning transmission electron microscope detection system was used at an operating voltage of 30 kV to observe the fine structures of nanoparticles. A transmission electron microscope (JEM-2100F, JEOL Ltd., Japan) was employed at an operating voltage of 200 kV to obtain high-resolution images of the synthesized nanoparticles. For scanning transmission electron microscopy (STEM) and transmission electron microscopy (TEM) observations, a droplet of the sample powder dispersed in ethanol solution was placed on a carbon-coated copper mesh grid and dried at room temperature. N<sub>2</sub> and water vapor gas adsorption–desorption measurements were employed to evaluate the pore structures (BELSORP-maxII, MicrotracBEL Corp., Japan). Prior to measurements, the sample powders were degassed at 200 °C for 6 h under vacuum condition. Gas adsorption tests were performed at 77 K (N<sub>2</sub>) and 298 K (water vapor). The pore size distribution was calculated using the adsorption profile by the Barrett–Joyner–Halenda (BJH) method. Fourier transform infrared spectroscopy (FT-IR; FT-720, HORIBA, Ltd., Japan) with the transmittance optical arrangement was used to determine the water content in the sample powder. The sample powders were dried at 40 °C for 24 h before measurement and were set in the cell equipped with a KRS-5 (mixed crystal of thallium bromo-iodide) window with a controlled thickness of 50 µm using an aluminum spacer. FT-IR with attenuated total reflectance (ATR) attachment with a diamond crystal (FT/IR-6600, JASCO Corp., Japan) was also used to characterize the chemical bonds of the synthesized samples. FT-IR ATR spectra were corrected with consideration of the penetration depth of the evanescent wave.

## 3. Results and Discussion

### 3.1. Shell-thickness control of HSNPs in ethanol-rich reaction conditions

Figure 1 shows the TEM image of pristine HSNP. The size of the particles was smaller than 100 nm without any coarse particles. The particles had a cubic or rectangular shape and hollow space in their insides. The statistically calculated outer particle diameter,  $d_{\text{outer}}$ , inner hollow diameter,  $d_{\text{inner}}$ , and shell thickness,  $t_{\text{shell}}$ , were 84 nm, 67 nm, and 10 nm, respectively. The hollow structure was further characterized by the N<sub>2</sub> adsorption–desorption technique (Fig. 2a). The isotherm was classified as type IV with a hysteresis loop of type H2b, which is a feature of materials with bottleneck-type pore structures.[32] The Brunauer-Emmett-Teller specific surface area of HSNPs was 296.7 m<sup>2</sup> g<sup>-1</sup>. The specific surface area was larger than the calculated value (106.0 m<sup>2</sup> g<sup>-1</sup>) using geometrical information from the TEM observation. This indicated that there were pores located in the shell matrix (intrapore pores). The pore-size distribution in area dimension showed a bimodal feature (Fig. 2b). The peak of the larger pore was positioned at 68.9 nm, which was in good agreement with  $d_{\text{inner}}$  observed by TEM. Another peak was located at 2.43 nm and there were a considerable number of pores smaller than 10 nm. These mesoscale pores were located at the intrapore, which contributed to increase the specific surface area larger than the calculated value. Figure 2c shows the water vapor adsorption–desorption isotherm. The area specific uptake amount of water vapor was calculated as 2.15 cm<sup>3</sup> m<sup>-2</sup>, which is larger than same-sized dense SiO<sub>2</sub> nanoparticles and comparable to the reported hollow SiO<sub>2</sub> nanoparticles.[10] This indicated that the intrapore pores worked as a channel to introduce water vapor, which significantly contributed to the total water uptake. Therefore, HSNPs used in this study have an advantage to confine water owing to both the inner hollow spaces and intrapore pores.

HSNPs were dispersed in water and degassed under vacuum condition to introduce water into the hollow spaces. Figure 3 shows the FT-IR ATR spectra of HSNP heat treated at 500 °C and after degassing in water. The bands at 3740 and 3640 cm<sup>-1</sup> were assigned to the isolated surface silanol group and weakly hydrogen bonded silanol group, respectively.[33,34]

Broad and weak bands at 3350 and 1640  $\text{cm}^{-1}$  of the pristine HSNPs were assigned to  $\nu(\text{O-H})$  and  $\delta(\text{H-O-H})$  vibrations, which were assumed as being from the remaining OH ligand and adsorbed water molecules. The bands at 1050 and 805  $\text{cm}^{-1}$  were assigned to asymmetric and symmetric  $\nu(\text{Si-O})$  vibrations.[35,36] The degassed powder showed increasing absorbance of the bands assigned to water molecules and the additional band at 950  $\text{cm}^{-1}$  assigned to  $\nu(\text{Si-OH})$  vibrations.[36,37] This indicated that liquid  $\text{H}_2\text{O}$  was successfully introduced and confined in the HSNPs. Considering a specific surface area of 296.7  $\text{m}^2 \text{g}^{-1}$  calculated by the  $\text{N}_2$  adsorption test and the molecular cross-sectional area of  $\text{H}_2\text{O}$  (0.125  $\text{nm}^2$ ), monolayer  $\text{H}_2\text{O}$  adsorbed on the outer/inner surface of HSNPs was calculated as 88.3  $\text{cm}^3 \text{g}^{-1}$ , which corresponded to 14% of the total adsorbed amount of water. Although the peak around 1050–1250  $\text{cm}^{-1}$  was sensitive to the chemical environment of silicon,[38] there was no significant shift. This implied that the chemical bonds were not affected by the introduction of water.

Water-containing HSNPs were redispersed in ethanol mixed with basic solution. It is known that the hydrolysis and condensation reactions of silicon alkoxides tend to proceed with well-polymerized siloxane species (in this study HSNPs) under basic conditions.[39] Tetraethyl orthosilicate was added to the water-containing HSNP suspension and a reaction was allowed for 20 h. Figure 4 shows the SEM and TEM images of the reacted nanoparticles. Although highly aggregated coarse particles were not observed (Fig. 4a), there were two types of nanoparticles; 1)  $d_{\text{outer}}$  of ~110 nm,  $d_{\text{inner}}$  of ~65 nm, and  $t_{\text{shell}}$  of ~23 nm (indicated by a red arrow in Fig. 4b); 2)  $d_{\text{outer}}$  of ~110 nm,  $d_{\text{inner}}$  of ~28 nm, and  $t_{\text{shell}}$  of ~41 nm (indicated by a blue arrow in Fig. 4b). The former particles were larger than pristine HSNPs without a size change of the inner hollow space, which indicated that added TEOS reacted at the surface of the HSNPs to grow the shells. However, the latter particles showed a larger outer particle diameter and smaller inner hollow space than pristine HSNPs. This meant that TEOS molecules penetrated and diffused into the inner space of the HSNPs. Shell growth in the



inwards direction decreased the confined water content and limited the advantage of the hollow structures. While several synthetic parameters of reaction temperature, concentrations of HSNPs and TEOS, and additives were tuned to avoid progress of such an inhomogeneous reaction, it was hard to prevent the growth of the shell in the inwards direction. Therefore, the reaction environment was drastically changed, as reported in the next section.

### 3.2. Shell-thickness control of HSNPs in water-rich reaction conditions

In this section, a water-rich environment is employed instead of the ethanol-rich environment in the previous section. Figure 5a–5e shows the STEM images of TEOS-*y*. Homogeneous hollow structures were observed for the cases of TEOS-1.73, TEOS-2.60, TEOS-3.46, and TEOS-4.33. TEOS-6.50 showed dense small nanoparticles (diameter < 50 nm) in addition to HSNPs. It was deduced that the small dense nanoparticles formed as a result of hydrolysis and condensation of TEOS irrespective of the HSNPs. The condensation reaction will preferentially take place on the surface of HSNPs considering the relatively stronger electron withdrawing characteristic of the –OSi ligand than the –OC<sub>2</sub>H<sub>5</sub> and –OH ligands.[39] However, the addition of an excess amount of TEOS will allow progress of the condensation reaction with a poorly condensed species and formation of nanoparticles in addition to HSNPs. Figures 6a and S1 show the size change of  $d_{\text{outer}}$  and  $d_{\text{inner}}$  depending on the TEOS amounts. The  $d_{\text{outer}}$  increased with TEOS amount, in contrast, the  $d_{\text{inner}}$  were almost comparable. This indicated that HSNPs grew in the outward direction rather than the inward direction. The approach using a water-rich environment was successful to control the  $t_{\text{shell}}$  of HSNPs without losing the hollow space. Subsequently, the water-rich environment was employed with different types of silicon alkoxides, the TMOS-*y*, TPOS-*y*, and TBOS-*y* systems. The  $d_{\text{outer}}$  and  $d_{\text{inner}}$  are shown in Figure S2. The  $d_{\text{inner}}$  were comparable to that of pristine HSNPs except for TBOS-4.33. It was assumed that the HSNPs showed growth in the outward direction even when different alkoxides were used.

The microscopic observation indicated a different tendency of reaction depending on the alkoxides. In the case of TMOS-y, dense nanoparticles started to be observed with a smaller amount of alkoxide (3.46 mmol) compared with the TEOS-y system (Fig. 5f). The TPOS-y system did not show any dense nanoparticles up to 4.33 mmol of alkoxide (Fig. 5g). TBOS-4.33 showed the formation of small dense nanoparticles (Fig. 5h). Figure 6b summarizes that  $t_{\text{shell}}$  of HSNPs reacted with different amounts of TMOS, TEOS, TPOS, and TBOS. The  $t_{\text{shell}}$  increased by increasing the amount of alkoxide with different tendencies. The  $t_{\text{shell}}$  gradually increased for the systems of TEOS-y and TPOS-y. The TMOS-y system showed a gradual increase and decrease, which might have arisen from the formation of a significant amount of dense silica particles. In the case of the TBOS-y system,  $t_{\text{shell}}$  rapidly increased. These differences were assumed to be derived from the differing reactivities of the alkoxides. The solubility of each alkoxide in ethanol was sufficiently high and a large amount of ethanol (alkoxide:ethanol = 1:100 (molar ratio)) improved the miscibility in a water-rich environment,[39] which allowed for a homogeneous reaction. A depolymerization reaction will take place in basic conditions, but this will be efficiently retarded by the addition of alcohol.[40] Therefore, it was deduced that the hydrolysis and condensation reactions proceeded with a significantly slow reverse reaction in this study. It has been reported that substitution of the ethoxide ligand to a methoxide ligand in TEOS accelerates the hydrolysis reaction owing to the inductive effect.[41,42] Hence, in this study, the stronger basicity of the methoxide ligand compared with the ethoxide ligand improved the hydrolysis reaction and enabled the formation of nanoparticles with smaller amounts of alkoxide. In the case of TBOS, the steric effect significantly increases.[43,44] Although transesterification with ethanol will occur, the reaction rate will still be small,[45,46] which indicates that the hydrolysis and condensation reactions of TBOS will likely result in a more reaction-limited mechanism different from the other systems. This hinders the reaction progress on the surface

of HSNPs and improves the formation of dense nanoparticles as a result of condensation between molecular species.

Figure 7a shows the transmittance IR spectra of pristine HSNPs, water, and TEOS- $y$  ( $y = 1.73\text{--}4.33$ ), with a measurement length of 50  $\mu\text{m}$ . The HSNPs were heat treated at 40  $^{\circ}\text{C}$  for 24 h before the measurement. The spectrum of water indicated that the FIR light with wavenumbers around  $3700\text{--}3000\text{ cm}^{-1}$  (wavelength of  $2.70\text{--}3.33\text{ }\mu\text{m}$ ) was fully absorbed with a 50- $\mu\text{m}$ -thick water layer. In the case of the TEOS- $y$  system, the transmittance of the FIR light decreased by increasing the TEOS amount. Considering that the  $t_{\text{shell}}$  increased with the TEOS amount, the FIR transmittance of TEOS- $y$  depended on the  $t_{\text{shell}}$ . The relationship between  $t_{\text{shell}}$  and FIR transmittance is shown in Fig. 7b. The trend was comparable in all systems; the FIR transmittance decreased with increasing  $t_{\text{shell}}$ . The transmittance decreased to  $\sim 10\%$  when the  $t_{\text{shell}}$  was approximately 30 nm. This clearly indicated that the confinement and retention of water in hollow space of HSNPs was precisely controlled by tuning the thickness of the shells.

#### 4. Conclusion

In this study, shell thickness of hollow silica nanoparticles was controlled through post-treatment by the sol-gel technique. In the case of ethanol-rich base conditions, the hydrolysis reaction and condensation reaction of TEOS took place around the surface of silica nanoparticles. However, the shells grew in the inward direction as well as the outward direction, which limited the inner hollow space and the corresponding functions. We found that growth control of the shells was successful when water-rich conditions were employed. Tuning the synthetic conditions of the ligand structure and concentration of silicon alkoxides enabled the formation of water-confined silica nanoparticles, *i.e.*, nanocomposites, with a controlled thickened shell. The confined water was retained efficiently even after heating at 40  $^{\circ}\text{C}$  for 24 h by increasing the shell thickness. The water-confined silica nanoparticles are expected to be used as efficient visible-light transparent FIR absorbers in various applications,

such as smart windows and cosmetics. Moreover, the facile confinement approach shown in this study will lead to highly functional complex nanocomposites, such as isolated metal nanoparticles–water–silica.

### **CRedit authorship contribution statement**

Study design: N. Tarutani, T. Uchikoshi, T. Ishigaki; Experimental analyses: N. Tarutani, Y. Honda, R. Hamakawa; Data evaluation: N. Tarutani, Y. Honda, R. Hamakawa. All authors read and approved the final version of the manuscript.

### **Declaration of Competing Interest**

The authors declare that there is no conflict of interest.

### **Acknowledgements**

The present work is partially supported by JSPS KAKENHI Grant Number JP20K15368, MEXT Leading Initiative for Excellent Young Researchers, the Foundation for the Promotion of Ion Engineering, and the Izumi Science and Technology Foundation (2019-J-112). We thank Edanz (<https://jp.edanz.com/ac>) for editing a draft of this manuscript.

### **References**

- [1] C. Sanchez, B. Julián, P. Belleville, M. Popall, Applications of hybrid organic-inorganic nanocomposites, *J. Mater. Chem.* 15 (2005) 3559–3592. <https://doi.org/10.1039/b509097k>.
- [2] Z. Wang, L. Zhou, X.W. Lou, Metal oxide hollow nanostructures for lithium-ion batteries, *Adv. Mater.* 24 (2012) 1903–1911. <https://doi.org/10.1002/adma.201200469>.
- [3] Y. Yao, M.T. McDowell, I. Ryu, H. Wu, N. Liu, L. Hu, W.D. Nix, Y. Cui, Interconnected silicon hollow nanospheres for lithium-ion battery anodes with long cycle life, *Nano Lett.* 11 (2011) 2949–2954. <https://doi.org/10.1021/nl201470j>.
- [4] S. Mondal, Phase change materials for smart textiles - An overview, *Appl. Therm. Eng.* 28 (2008) 1536–1550. <https://doi.org/10.1016/j.applthermaleng.2007.08.009>.
- [5] J.F. Li, Y.F. Huang, Y. Ding, Z.L. Yang, S.B. Li, X.S. Zhou, F.R. Fan, W. Zhang, Z.Y. Zhou, D.Y. Wu, B. Ren, Z.L. Wang, Z.Q. Tian, Shell-isolated nanoparticle-enhanced

- Raman spectroscopy, *Nature*. 464 (2010) 392–395.  
<https://doi.org/10.1038/nature08907>.
- [6] C. Graf, A. Van Blaaderen, Metallodielectric colloidal core-shell particles for photonic applications, *Langmuir*. 18 (2002) 524–534. <https://doi.org/10.1021/la011093g>.
- [7] F. Caruso, R.A. Caruso, H. Möhwald, Nanoengineering of inorganic and hybrid hollow spheres by colloidal templating, *Science*. 282 (1998) 1111–1114.  
<https://doi.org/10.1126/science.282.5391.1111>.
- [8] I. Tissot, C. Novat, F. Lefebvre, E. Bourgeat-Lami, Hybrid Latex Particles Coated with Silica, *Macromolecules*. 34 (2001) 5737–5739. <https://doi.org/10.1021/ma010278r>.
- [9] E. Bourgeat-Lami, I. Tissot, F. Lefebvre, Synthesis and Characterization of SiOH-Functionalized Polymer Latexes Using Methacryloxy Propyl Trimethoxysilane in Emulsion Polymerization, *Macromolecules*. 35 (2002) 6185–6191.  
<https://doi.org/10.1021/ma012230j>.
- [10] M. Fuji, C. Takai, Y. Tarutani, T. Takei, M. Takahashi, Surface properties of nanosize hollow silica particles on the molecular level, *Adv. Powder Technol.* 18 (2007) 81–91.  
<https://doi.org/10.1163/156855207779768124>.
- [11] M. Fuji, T. Shin, H. Watanabe, T. Takei, Shape-controlled hollow silica nanoparticles synthesized by an inorganic particle template method, *Adv. Powder Technol.* 23 (2012) 562–565. <https://doi.org/10.1016/j.appt.2011.06.002>.
- [12] R. V. Rivera Virtudazo, H. Tanaka, H. Watanabe, M. Fuji, T. Shirai, Facile preparation in synthesizing nano-size hollow silicate particles by encapsulating colloidal-hydroxyapatite nanoparticles, *J. Mater. Chem.* 21 (2011) 18205–18207.  
<https://doi.org/10.1039/c1jm14520g>.
- [13] Y. Sun, B.T. Mayers, Y. Xia, Template-Engaged Replacement Reaction: A One-Step Approach to the Large-Scale Synthesis of Metal Nanostructures with Hollow Interiors, *Nano Lett.* 2 (2002) 481–485. <https://doi.org/10.1021/nl025531v>.

- [14] B. Wang, H. Wu, L. Yu, R. Xu, T.T. Lim, X.W. Lou, Template-free formation of uniform urchin-like  $\alpha$ -FeOOH hollow spheres with superior capability for water treatment, *Adv. Mater.* 24 (2012) 1111–1116.  
<https://doi.org/10.1002/adma.201104599>.
- [15] M. FUJI, Hollow particles as controlled small space to functionalize materials, *J. Ceram. Soc. Japan.* 123 (2015) 835–844. <https://doi.org/10.2109/jcersj2.123.835>.
- [16] L. Yang, J.J. Bian, H. Zhang, X.R. Niu, G.F. Wang, Size-dependent deformation mechanisms in hollow silicon nanoparticles, *AIP Adv.* 5 (2015) 1–8.  
<https://doi.org/10.1063/1.4927509>.
- [17] Z. Jia, Z. Wang, D. Hwang, L. Wang, Prediction of the Effective Thermal Conductivity of Hollow Sphere Foams, *ACS Appl. Energy Mater.* 1 (2018) 1146–1157.  
<https://doi.org/10.1021/acsaem.7b00264>.
- [18] H. Geng, W. Chen, Z.P. Xu, G. Qian, J. An, H. Zhang, Shape-Controlled Hollow Mesoporous Silica Nanoparticles with Multifunctional Capping for In Vitro Cancer Treatment, *Chem. - A Eur. J.* 23 (2017) 10878–10885.  
<https://doi.org/10.1002/chem.201701806>.
- [19] Y. Sun, B. Mayers, Y. Xia, Metal Nanostructures with Hollow Interiors, *Adv. Mater.* 15 (2003) 641–646. <https://doi.org/10.1002/adma.200301639>.
- [20] C. Takai-Yamashita, M. Fuji, Hollow silica nanoparticles: A tiny pore with big dreams, *Adv. Powder Technol.* 31 (2020) 804–807. <https://doi.org/10.1016/j.appt.2019.11.034>.
- [21] E.G. Solveyra, E. De La Llave, V. Molinero, G.J.A.A. Soler-Illia, D.A. Scherlis, Structure, dynamics, and phase behavior of water in TiO<sub>2</sub> nanopores, *J. Phys. Chem. C.* 117 (2013) 3330–3342. <https://doi.org/10.1021/jp307900q>.
- [22] M.H. Factorovich, E. Gonzalez Solveyra, V. Molinero, D.A. Scherlis, Sorption isotherms of water in nanopores: Relationship between hydrophobicity, adsorption

- pressure, and hysteresis, *J. Phys. Chem. C*. 118 (2014) 16290–16300.  
<https://doi.org/10.1021/jp5000396>.
- [23] M.I. Velasco, M.B. Franzoni, E.A. Franceschini, E. Gonzalez Solveyra, D. Scherlis, R.H. Acosta, G.J.A.A. Soler-Illia, Water Confined in Mesoporous TiO<sub>2</sub> Aerosols: Insights from NMR Experiments and Molecular Dynamics Simulations, *J. Phys. Chem. C*. 121 (2017) 7533–7541. <https://doi.org/10.1021/acs.jpcc.6b12511>.
- [24] W. Suthabanditpong, C. Takai, M. Fuji, R. Bunttem, T. Shirai, Improved optical properties of silica/UV-cured polymer composite films made of hollow silica nanoparticles with a hierarchical structure for light diffuser film applications, *Phys. Chem. Chem. Phys.* 18 (2016) 16293–16301. <https://doi.org/10.1039/c6cp01005a>.
- [25] N. Terada, K. Ohnishi, M. Kobayashi, T. Kunitomo, Spectral radiative properties of a living human body, *Int. J. Thermophys.* 7 (1986) 1101–1113.  
<https://doi.org/10.1007/BF00502381>.
- [26] L.W. Pinkley, P.P. Sethna, D. Williams, Optical constants of water in the infrared, *J. Opt. Soc. Am.* 67 (1977) 494. <https://doi.org/10.1364/JOSA.67.000494>.
- [27] H. Döschner, J.F. Geisz, T.G. Deutsch, J.A. Turner, Sunlight absorption in water-efficiency and design implications for photoelectrochemical devices, *Energy Environ. Sci.* 7 (2014) 2951–2956. <https://doi.org/10.1039/c4ee01753f>.
- [28] T.A. Cooper, S.H. Zandavi, G.W. Ni, Y. Tsurimaki, Y. Huang, S. V. Boriskina, G. Chen, Contactless steam generation and superheating under one sun illumination, *Nat. Commun.* 9 (2018) 1–10. <https://doi.org/10.1038/s41467-018-07494-2>.
- [29] M. Fuji, T. Shin, H. Watanabe, T. Takei, Shape-controlled hollow silica nanoparticles synthesized by an inorganic particle template method, *Adv. Powder Technol.* 23 (2012) 562–565. <https://doi.org/10.1016/j.appt.2011.06.002>.

- [30] J.H. Park, S.Y. Bae, S.G. Oh, Fabrication of hollow silica microspheres through the self-assembly behavior of polymers in W/O emulsion, *Chem. Lett.* 32 (2003) 598–599. <https://doi.org/10.1246/cl.2003.598>.
- [31] D. Cheng, X. Zhou, H. Xia, H.S.O. Chan, Novel Method for the Preparation of Polymeric Hollow Nanospheres Containing Silver Cores with Different Sizes, *Chem. Mater.* 17 (2005) 3578–3581. <https://doi.org/10.1021/cm0503230>.
- [32] M. Thommes, K.A. Cychosz, Physical adsorption characterization of nanoporous materials: Progress and challenges, *Adsorption*. 20 (2014) 233–250. <https://doi.org/10.1007/s10450-014-9606-z>.
- [33] R.S. McDonald, Surface functionality of amorphous silica by infrared spectroscopy, *J. Phys. Chem.* 62 (1958) 1168–1178. <https://doi.org/10.1021/j150568a004>.
- [34] H.A. Benesi, A.C. Jones, An infrared study of the water-silica gel system, *J. Phys. Chem.* 63 (1959) 179–182. <https://doi.org/10.1021/j150572a012>.
- [35] J. BOCK, G. -J SU, Interpretation of the Infrared Spectra of Fused Silica, *J. Am. Ceram. Soc.* 53 (1970) 69–73. <https://doi.org/10.1111/j.1151-2916.1970.tb12012.x>.
- [36] A. Duran, C. Serna, V. Fornes, J.M. Fernandez Navarro, Structural considerations about SiO<sub>2</sub> glasses prepared by sol-gel, *J. Non. Cryst. Solids.* 82 (1986) 69–77. [https://doi.org/10.1016/0022-3093\(86\)90112-2](https://doi.org/10.1016/0022-3093(86)90112-2).
- [37] D. Niznansky, J.L. Rehspringer, Infrared study of SiO<sub>2</sub> sol to gel evolution and gel aging, *J. Non. Cryst. Solids.* 180 (1995) 191–196. [https://doi.org/10.1016/0022-3093\(94\)00484-6](https://doi.org/10.1016/0022-3093(94)00484-6).
- [38] J.E. Olsen, F. Shimura, Infrared spectroscopy of thin silicon dioxide on silicon, *Appl. Phys. Lett.* 53 (1988) 1934–1936. <https://doi.org/10.1063/1.100487>.
- [39] C.J. Brinker, G.W. Scherer, *Sol-Gel Science: The Physics and Chemistry of Sol-Gel Processing*, 2013. <https://doi.org/10.1016/C2009-0-22386-5>.



- [40] R.K. Iler, *The Chemistry of Silica: Solubility, Polymerization, Colloid and Surface Properties and Biochemistry of Silica*, Wiley, 1979. [https://doi.org/10.1016/S0301-4770\(08\)60805-2](https://doi.org/10.1016/S0301-4770(08)60805-2).
- [41] H. Schmidt, H. Scholze, A. Kaiser, Principles of hydrolysis and condensation reaction of alkoxysilanes, *J. Non. Cryst. Solids*. 63 (1984) 1–11. [https://doi.org/10.1016/0022-3093\(84\)90381-8](https://doi.org/10.1016/0022-3093(84)90381-8).
- [42] C.J. Brinker, Hydrolysis and condensation of silicates: Effects on structure, *J. Non. Cryst. Solids*. 100 (1988) 31–50. [https://doi.org/10.1016/0022-3093\(88\)90005-1](https://doi.org/10.1016/0022-3093(88)90005-1).
- [43] M.G. Voronkov, V.P. Mileshekevich, Y.A. Yuzhelevskii, *The siloxane bond : physical properties and chemical transformations*, Consultants Bureau, New York, 1978. <https://doi.org/10.1080/00945717908069783>.
- [44] R. Aelion, A. Loebel, F. Eirich, Hydrolysis of Ethyl Silicate, *J. Am. Chem. Soc.* 72 (1950) 5705–5712. <https://doi.org/10.1021/ja01168a090>.
- [45] C.. Brinker, K.. Keefer, D.. Schaefer, C.. Ashley, Sol-gel transition in simple silicates, *J. Non. Cryst. Solids*. 48 (1982) 47–64. [https://doi.org/10.1016/0022-3093\(82\)90245-9](https://doi.org/10.1016/0022-3093(82)90245-9).
- [46] C.J. Brinker, K.D. Keefer, D.W. Schaefer, R.A. Assink, B.D. Kay, C.S. Ashley, Sol-gel transition in simple silicates II, *J. Non. Cryst. Solids*. 63 (1984) 45–59. [https://doi.org/10.1016/0022-3093\(84\)90385-5](https://doi.org/10.1016/0022-3093(84)90385-5).

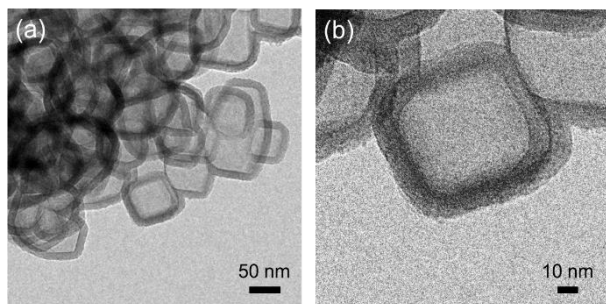


**Fig. 1** TEM images of pristine HSNP. (b) A magnified image of a section in (a).

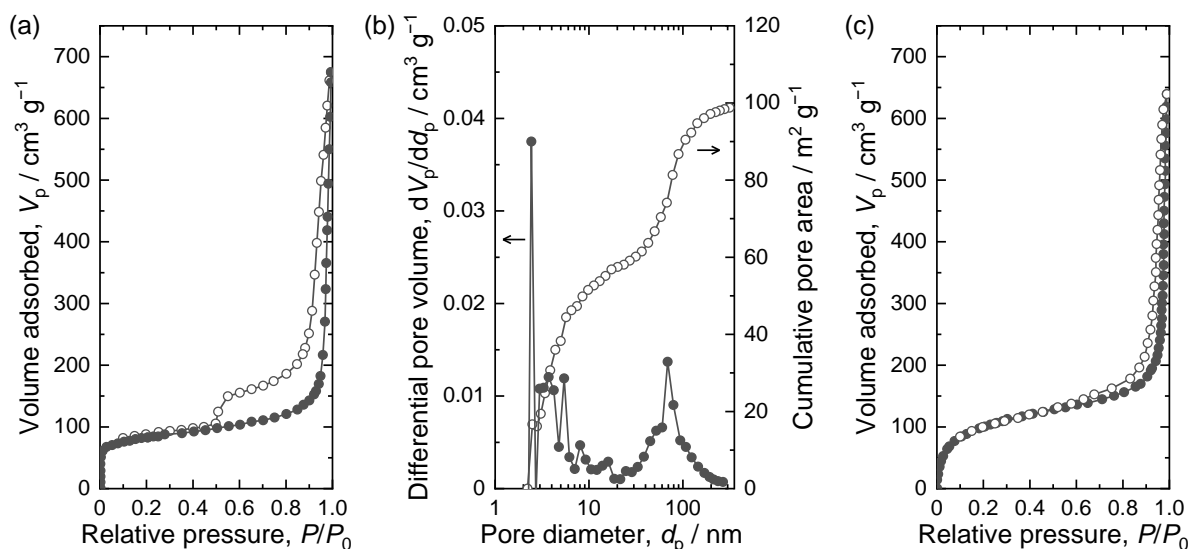


**Fig. 2** (a) Nitrogen adsorption–desorption isotherm, (b) pore size distribution in area dimension, and (c) water adsorption–desorption isotherm of pristine HSNPs.

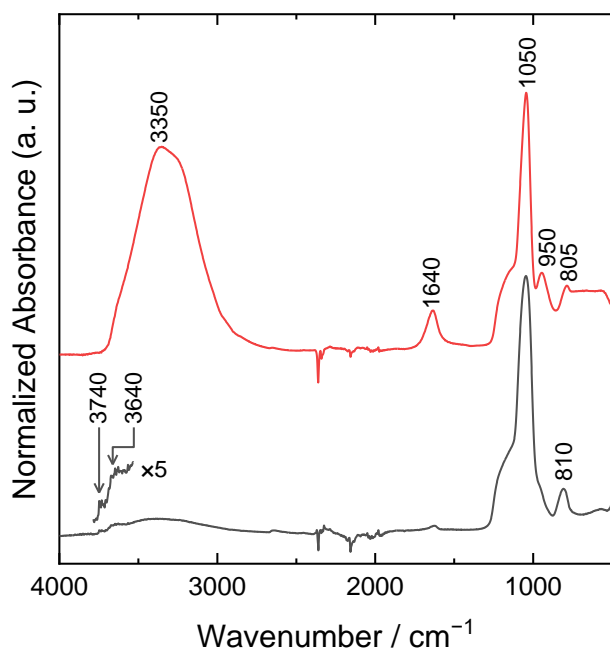


**Fig. 3** FT-IR ATR spectra of pristine (black) and water-containing (red) HSNPs.

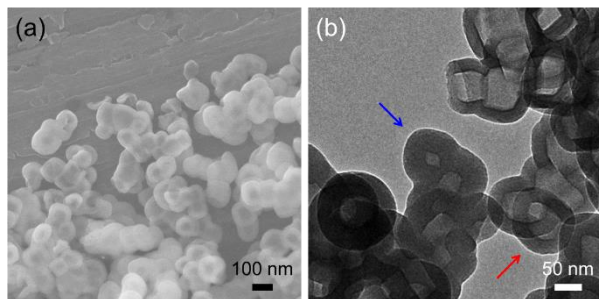


**Fig. 4** (a) SEM and (b) TEM images of HSNPs reacted with TEOS in ethanol-rich conditions. Red and blue arrows indicate the HSNP having comparable and smaller inner space than pristine HSNPs, respectively.

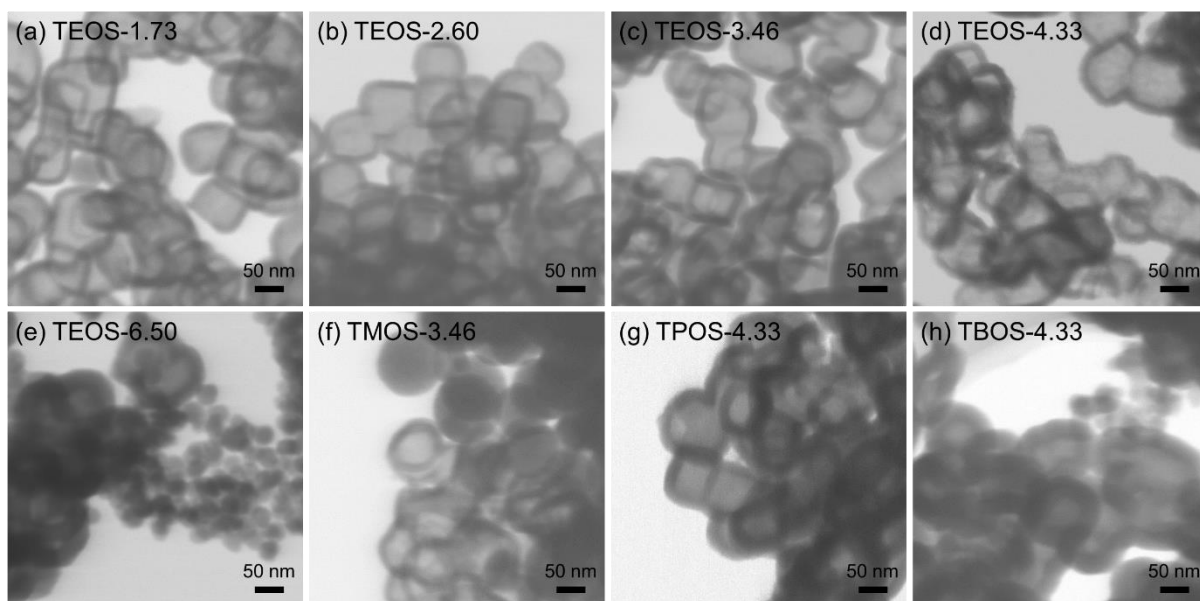


**Fig. 5** STEM images of (a) TEOS-1.73, (b) TEOS-2.60, (c) TEOS-3.46, (d) TEOS-4.33, (e) TEOS-6.50, (f) TMOS-3.46, (g) TPOS-4.33, and (h) TPOS-4.33.

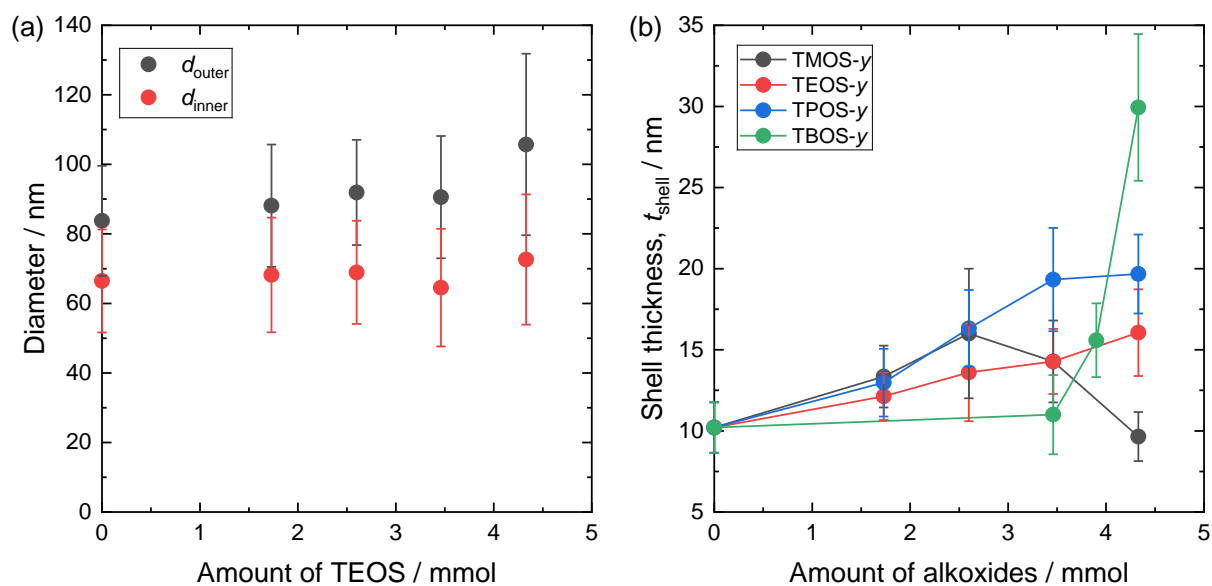


**Fig. 6** (a) The  $d_{outer}$  (black) and  $d_{inner}$  (red) of TEOS- $y$  ( $y = 1.73$ – $4.33$ ) and (b) the  $t_{shell}$  of TMOS- $y$  (black), TEOS- $y$  (red), TPOS- $y$  (blue), and TBOS- $y$  (green) ( $y = 1.73$ – $4.33$ ) with those of pristine HSNPs. The  $d_{outer}$ ,  $d_{inner}$ , and  $t_{shell}$  of 100 particles are averaged.

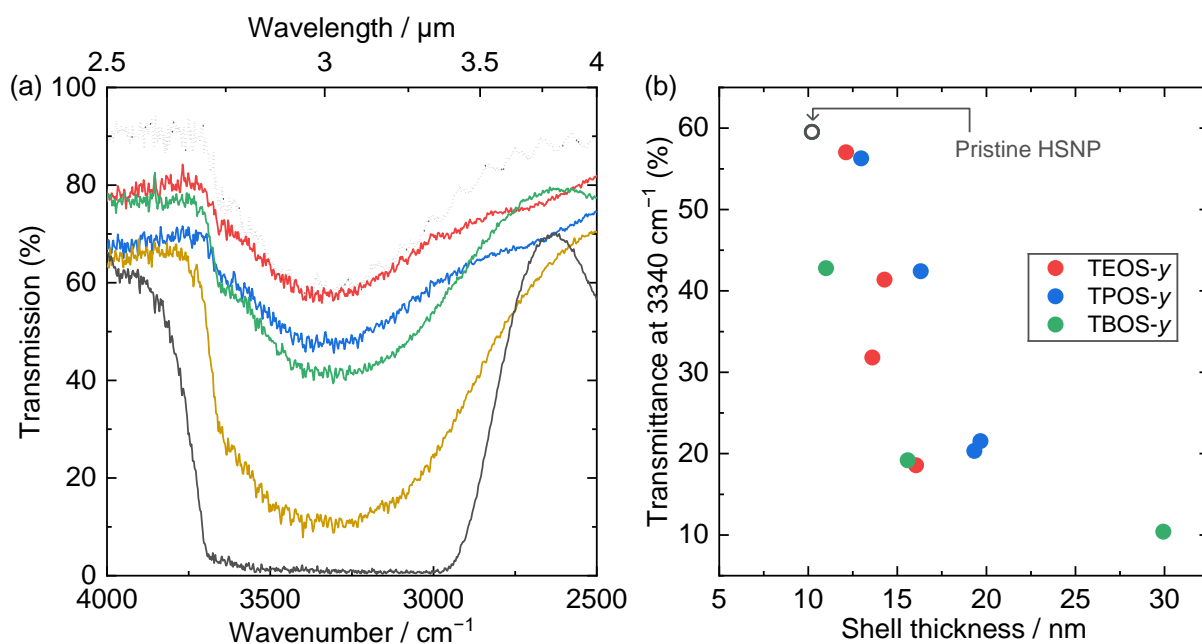


**Fig. 7** (a) FIR transmittance spectra of pristine HSNP (dot), water (black), TEOS-1.73 (red), TEOS-2.60 (blue), TEOS-3.46 (green), and TEOS-4.33 (yellow) with a controlled sample thickness of 50  $\mu\text{m}$  using an aluminum spacer. (b) The  $t_{\text{shell}}$  dependent change of FIR transmittance at 3340  $\text{cm}^{-1}$ .